Manuscript Details

Manuscript number	MSEC_2018_865
Title	Rapid Nano-Scale Surface Modification on Micro-Arc Oxidation Coated Titanium by Microwave Assisted Hydrothermal Process
Article type	Research Paper

Abstract

Nano to submicron scaled surface possesses excellent biological affinity and several processes have been undertaken to develop titanium implant with specific surface chemical and phase composition and nanoscale features. We use a simple microwave process to modify the nano topographies on a micro-arc-oxidation (MAO) surface which shortens the time for conventional hydrothermal process (HT). Nano-scaled anatase precipitates on the MAO surface with different crystallinities and morphologies were regulated via microwave assisted hydrothermal in pure water (MWDD) or in pH conditioned mediums containing calcium and phosphorus ions (MWCP, MWCP9, MWCP11). The surface morphologies and structures were investigated by SEM, XRD, FTIR, and TEM. Pyramid and rod-like anatase nanocrystals along [0 0 1] direction were observed on the surface of the MWDD and MWCP groups. Increasing the pH of the conditioned mediums lead the precipitates to lose its crystallinity; the surface of MWCP11 is covered with amorphous anatase which has a 3D nano-sheet architecture. The nano-featured surfaces adsorb more proteins (fibronectin and bovine serum albumin), and the osteoblasts like MG63 cells spreading on these surfaces were faster than that on the MAO and HT groups. Higher viability and alkaline phosphate activity were found in cells direct cultured on those MW groups than that on the MAO and HT groups on the 7th day. The microwave assisted hydrothermal processed MAO surfaces, which possess nano scale topography combined with micron/submicron pores are expected to adsorb more proteins and conduct the osteoblasts cells adherent, thus could enhance cell proliferation and cell differentiation to facilitate osseointegration without compromising the bonding strength.

Keywords	titanium implant; micro-arc oxidation; nano topography; surface modification; hydrothermal; microwave irradiation
Taxonomy	Materials Characterization Techniques, Materials Structure

Corresponding Author	Dan-Jae Lin
Corresponding Author's Institution	-
Order of Authors	Dan-Jae Lin, Lih-Jyh Fuh, Cheng-Yu Chen, Wen-Cheng Chen, Jiin-Huey Chern Lin, Chiing-Chang Chen

Suggested reviewers	Takao Hanawa, John Hunt, Her-Hsiung Huang

Submission Files Included in this PDF

File Name [File Type]

cover letter.docx [Cover Letter]

Highlights.docx [Highlights]

Graphical Abstract.tif [Graphical Abstract]

20180315-new.docx [Manuscript File]

Supplementary.docx [Supporting File]

To view all the submission files, including those not included in the PDF, click on the manuscript title on your EVISE Homepage, then click 'Download zip file'.

Professor Michelle Oyen
Editor-in-Chief
University of Cambridge, Cambridge, England, UK

Mar 26, 2018

Dear Professor Oyen:

I am submitting a manuscript, entitled "**Rapid Nano-Scale Surface Modification on Micro-Arc Oxidation Coated Titanium by Microwave-Assisted Hydrothermal Process**", for your consideration for publication in the journal "Materials Science & Engineering C: Materials for Biological Applications".

This original research reported in this manuscript is a latest cooperation research contributed by specialists from fields including, Materials sciences (Prof. Wen-Cheng Chen and I), Dentistry (Prof. Dr. Fuh) and Chemistry (Prof. Chen CC). It has been partially funded through the National Science Council, Taiwan, R.O.C. (NSC 101-2320-B-039-004-MY3; MOST 105-2314-B-039-046-MY2). The data used in this manuscript is not under consideration for publication elsewhere. The publication is approved by all authors and that, if accepted, it will not be published elsewhere in the same form, in English or in any other language, without the written consent of the copyright-holder. I appreciate your time and effort on reviewing this work.

_____

(Signature of corresponding author on behalf of all authors)

Dan-Jae Lin
Associate Professor
Department of Dental Hygiene
School of Dentistry
China Medical University, No.91 Hsueh-Shih Road, Taichung, Taiwan 40402, R.O.C
Fax: +886 4 22073556
E-mail: djlin@mail.cmu.edu.tw

Highlights

1. Nano-scale topography on micro-arc-oxidation surfaces produced by rapid process.
2. The surface is super hydrophilicity with enhanced protein adsorption.
3. Promote MG63 cell adherent, enhancing cell proliferation and differentiation.

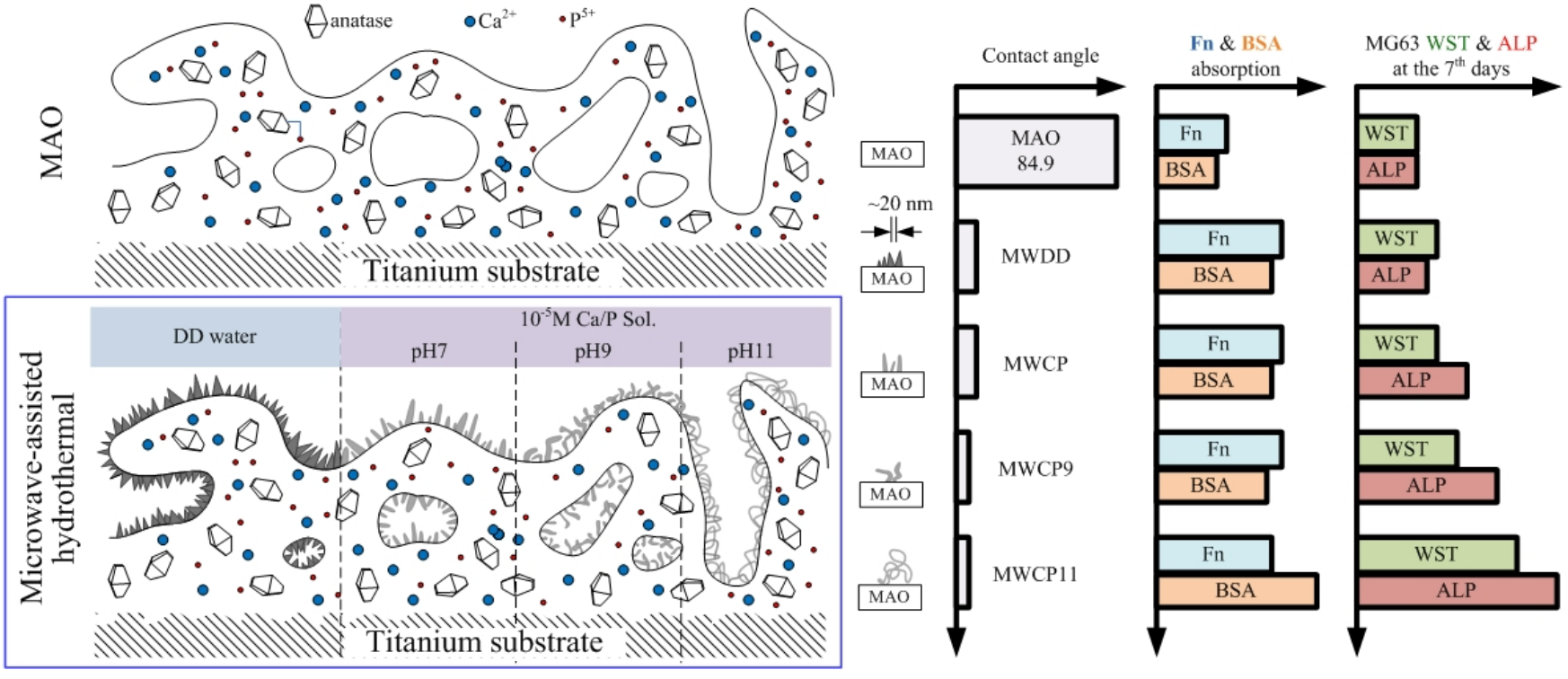
MAO
anatase
Ca^{2+}
P^{5+}
Titanium substrate
Microwave-assisted hydrothermal
DD water
10^{-5}M Ca/P Sol.
pH7
pH9
pH11
Titanium substrate
Contact angle
Fn & BSA absorption
MG63 WST & ALP at the 7th days
MAO
MAO 84.9
~20 nm
MWDD
MWCP
MWCP9
MWCP11
Fn
BSA
WST
ALP

Article

Rapid Nano-Scale Surface Modification on Micro-Arc Oxidation Coated Titanium by Microwave-Assisted Hydrothermal Process

Dan-Jae Lin [1,2,3,4] *, Lih-Jyh Fuh [1,2], Cheng-Yu Chen [3], Wen-Cheng Chen [5], Jiin-Huey Chern Lin [6], and Chiing-Chang Chen [7]

[1] Department of Dental Hygiene, China Medical University, Taichung, Taiwan, ROC; djlin@mail.cmu.edu.tw
[2] School of Dentistry, College of Dentistry, China Medical University, Taichung, Taiwan, ROC; ljfuh@mail.cmu.edu.tw
[3] Graduate Institute of Basic Medical Science, College of Medicine, China Medical University, Taichung, Taiwan, ROC; k55599911@hotmail.com
[4] Biomaterials Translational Research Center, China Medical University Hospital, Taichung, Taiwan, ROC; djlin@mail.cmu.edu.tw
[5] Advanced Medical Devices and Composite Laboratory, Department of Fiber and Composite Materials, Feng Chia University, Taichung, Taiwan, ROC; wencchen@mail.fcu.edu.tw
[6] Department of Materials Science and Engineering, National Cheng-Kung University, Tainan, Taiwan, ROC; chernlin@mail.ncku.edu.tw
[7] Department of Science Application and Dissemination, National Taichung University of Education, Taichung, Taiwan, ROC; ccchen@mail.ntcu.edu.tw

* Correspondence: djlin@mail.cmu.edu.tw; Tel.: +886-4-22053366 ext. 7706

Received: date; Accepted: date; Published: date

Abstract: Nano to submicron scaled surface possesses excellent biological affinity and several processes have been undertaken to develop titanium implant with specific surface chemical and phase composition and nanoscale features. We use a simple microwave process to modify the nano topographies on a micro-arc-oxidation (MAO) surface which shortens the time for conventional hydrothermal process (HT). Nano-scaled anatase precipitates on the MAO surface with different crystallinities and morphologies were regulated via microwave-assisted hydrothermal in pure water (MWDD) or in pH conditioned mediums containing calcium and phosphorus ions (MWCP, MWCP9, MWCP11). The surface morphologies and structures were investigated by SEM, XRD, FTIR, and TEM. Pyramid and rod-like anatase nanocrystals along [0 0 1] direction were observed on the surface of the MWDD and MWCP groups. Increasing the pH of the conditioned mediums lead the precipitates to lose its crystallinity; the surface of MWCP11 is covered with amorphous anatase which has a 3D nano-sheet architecture. The nano-featured surfaces adsorb more proteins (fibronectin and bovine serum albumin), and the osteoblasts-like MG63 cells spreading on these surfaces were faster than that on the MAO and HT groups. Higher viability and alkaline phosphate activity were found in cells direct cultured on those MW groups than that on the MAO and HT groups on the 7th day. The microwave-assisted hydrothermal processed MAO surfaces, which possess nano-scale topography combined with micron/submicron pores are expected to adsorb more proteins and conduct the osteoblasts cells adherent, thus could enhance cell proliferation and cell differentiation to facilitate osseointegration without compromising the bonding strength.

Keywords: titanium implant; micro-arc oxidation; nano topography; surface modification; hydrothermal; microwave irradiation

1. Introduction

Surface roughness and surface topography of titanium implant are positively associated with the successful osseointegration and bone healing process [1, 2]. In recent years, the importance of manipulating surface topography in micron, sub-micron, and nano-scale has been addressed intensely [3-6], among other materials factors such as chemical composition, phase structure, and mechanical properties. Hori et al. [7] detail an in

vitro study describing controlled modification of titanium surfaces at the micron level with the addition of predetermined nano-surface features and nano-roughness, producing enhanced cellular responses. Their study correlated increased osteoblast differentiation and enhanced osteoblast proliferation as a function of a combined "micron-to-nanoscale hierarchical structure." The nanoscale topography in combination with micro and sub-micro scale roughness improves osteoblast differentiation and EMC production, which indicates the potential for improved implant osseointegration in vivo [4, 7]. The nano-featured surface of biomaterials is believed to not only regulate cell behaver by adsorb proteins heterogeneously as functional ECM [5, 6] but also can stimulate the cell functions by mechanotransduction signaling pathways [6].

Micro-arc-oxidization (MAO) is a high temperature plasma fusion process. By increasing voltage between titanium (anode) and cathode, the titanium surface will generate a thick oxide which will later been breakdown and fuse again by plasma extrusion in a higher voltage (usually above 150V). The coating growth mechanism is influenced by electrolytes [8]. As a result a porous oxide layer comprises of amorphous and anatase/or rutile phases was produced on the surface of titanium, and the inter-connective pores and micro-scale roughness of the MAO layer would increase the extracellular matrix (ECM) adsorption, as well as improve the mechanical interlock between bony tissue and implants. Using electrolytes containing Ca and P performing MAO titanium makes the surface of titanium form a uniform porous titania layer possess Ca and P ions in the less crystalline region through [9], and these ions would diffuse from the anodic oxide to form amorphous Ca- and P-containing precipitate [10] or hydroxyapatite (HA) crystallites during further hydrothermal treatment to increasing their bioactivity [11, 12].

Hydrothermal processing is a well-established technique for synthesis of many materials, but the kinetic of crystallization is slow. Moreover, because the mechanism is based on the solid state diffusion and ion exchange of Ca, P ions to the solid-liquid interface during hydrothermal treatments, the size of HA crystallite is not easily to precious control over a uniform morphology of nano-scale [13]. Song et al. using MAO followed by HT in a relative lower temperature to obtained a nanosheet-shaped morphology (135°C), nano-needles (150°C) and nanorods (175°C) on the porous MAO surface [14]. They found the hydrophilicity dramatically increased as the hydrothermal temperature increased. However the osteoblastic cells were fail to adhesion onto the MAO surface with nano-needles and nanorods, and their viability are lower than that culture on the MAO surface without nano scale feature [14]. They concluded as nano-topology formed on micro porous oxide layer was more important than hydrophilicity in its effect upon initial osteoblastic cell functions. However the hydrothermal process is time consumed and they did not provide enough information about the phase structure of these nano-scale layer.

Li et al. using a two-step MAO process to produce a surface consisting of microslots (3–10 μm) and submicro/nanopores (80–200 nm) on the macropores (100–300 μm) MAO titanium [15]. They found the hydrophilicity of the MAO has been increased and improve the in-vitro bioactivity because of the macro/micro/nano triple hierarchical structure. It is well known that thick ceramic coatings (around 5–10 μm for MAO) will take a big risk in delamination after implantation in a load bearing site, i.e. dental implant into the mandibular bone or hip/knee replacement. However, the achieved researches barely including mechanical evaluations to their coatings.

In view of this, we introduce a new concept to modify the MAO surface using a commercial microwave reactor, which is used to chemical synthesis, acid digest for element analysis, hydrolysis, and drying. Microwave-assisted synthesis plied reaction to be done faster, simple and efficient method to prepare nano-size inorganic materials. Compared with conventional methods, microwave synthesis has the advantages in its application to rapid growth, products with small particle size and narrow particle size distribution. These characterizations were due to fast homogenous nucleation and microwave-nucleated samples have higher population of nuclei with smaller size than the samples nucleated by conventional heating [16, 17]. Microwaves play an important role in reactions in aqueous media and have been used for preparing various nano-sized particles, such as HA [18, 19]. The aim of this study is to create a nano-scale feature on porous titania layer of the MAO titanium surface by microwave/hydrothermal process in different conditioned medium and pH. The created nano- and micro-scale topographies on the outer layer of MAO were characterized by observing the morphologies and checking the phase structures and their hydrophilicity. The hydrophilicity of the surface may play also crucial to the adsorbing proteins. It has been suggest that plasma fibronectin binds more to hydrophilic surfaces [20], whereas albumin binds more to hydrophobic surfaces [21]. However the later study did not control the roughness in nano-scale nor measure the surface hydrophilicity. *In-vitro* study of protein adsorption can verify the bio-functions of the surface and hence to predict the bio-integration of biomaterials [22]. In this study, the protein adsorption analysis was performed with fibronectin (Fn) and bovine serum albumin (BSA). The cell

adherent, proliferation and differentiation of MG63 osteoblasts-like cells cultured on the nano-modified surface will also be evaluated.

2. Materials and Methods

2.1 Sample preparation

The MAO process was detailed in previous paper [23]. Briefly, commercially grade 2 pure titanium discs (12 mm in diameter and 1 mm in thickness) were mechanical/chemical polished and cleaned. The MAO process was performed at a galvanostatic mode by a DC power supply under a constant current density of 10 mA/cm^2 to achieve a final voltage of 280 V for 3 minutes. The electrolytes composed of 0.2 M calcium acetate and 0.04 M β-glycerol phosphate disodium. The MAO titanium discs were microwave irradiated using a MARS 5 microwave reaction system with XP-1500 vessels (MARS 5, CEM, Matthews, NC, USA) at 2.45 GHz, 400 W. The maximum temperature was set at 200°C with a heating rate of 10 °C/min and the temperature was held at 200°C for 1 minute. The microwave process is illustrated in Figure 1. The MAO samples were immersed in the vessels containing 50 mL of double distilled water under microwave irradiation as describe above (MWDD group). For the MWCP groups, the Ca/ P ions in solution was consisted of 0.05 mM calcium hydroxide and 0.03 mM ammonium dihydrogen phosphate (MWCP), and the same Ca/P ions in solution with pH value adjust to pH 9.6 (MWCP9), pH 11 (MWCP11) for 30 minutes were compared. The MAO-hydrothermal treated samples (HT) were prepared by a MAO sample in a custom made hydrothermal device (stainless steel container with a 100 mL Teflon inlayer) containing 50 mL of double distilled water under 250°C for 2.5 hr. The specimens were ultrasonic cleaned with double distilled water twice and vacuum dried before the analysis. The specimens for biological evaluations were UV irradiated for 24 hr before the tests.

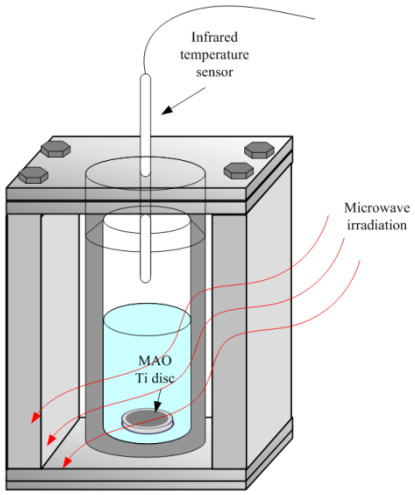

Figure 1. Illustration of microwave process using in this study. Micro-arc-oxidation titanium discs were put in a vessel containing conditioned medium (water or Ca/P solutions with adjusted pH) and irradiated with microwave at 2.45GHz, 400W (MARS 5, CEM) under controlled temperature (using an IR sensor).

2.2 Characterization of the coating

2.2.1 Surface morphology and composition

The surface morphologies of titanium samples were observed by a scanning electron microscopy equipped with an energy dispersive x-ray spectrometer (SEM/EDS, JSM-6300, JEOL Ltd., Tokyo, Japan). The composition of the sample was analyzed by energy dispersive spectra (EDS) from the entire scan area under magnification of 100x. The Kα peaks of O, P, Ca, and Ti were selected for analysis the atomic percentages of elements. The Ca and P concentration of crystalline phase on HT samples were detected using point analysis.

2.2.2 Phase structure

To analysis the crystallized product phases on the sample surfaces, we used a grazing-incidence X-ray diffractometry (In-plane GID, BRUKER D8 Discover, Germany) with Cu-Kα radiation (λ = 0.154 nm) at 40 kV and 40 mA. The XRD tests were conducted using a step scan, in which the angle (2θ) was set between 20° and 42° with incidence 1° and scanning velocity 0.02 step/3s. The phases of the compounds based on XRD analysis will be compared to the Joint Committee on Powder Diffraction Standards (JCPDS) files. Using JCPDS no. 21-1272, no. 44-1294, and no. 9-432 for identifying anatase, titanium, and hydroxyapatite, respectively. Fourier transform infrared spectrometer (FTIR) spectra were measured on a spectrophotometer (FTIR 460, Jasco Co., Tokyo, Japan) and transmission spectra of the samples were obtained by powder (obtained from peer of the MAO coating layer by bending 5 disc samples) mix with KBr (1:100 w/w) forming a thin transparent pellet.

2.2.3 Transmission Electron Microscopy (TEM)

The nano-scale precipitates on the MAO surface were investigated using a field emission transmission electron microscope (FE-TEM, JEM-2100F, JEOL, Japan) equipped with an energy dispersive x-ray spectroscopy (EDS, X-MaxN TSR, OXFORD). The specimens were prepared by powder method, briefly, debris were obtained from delamination by bending the disc samples. The debris of the MAO coating layer were dispersed in ethanol and then collected by a 300 grid copper mesh. Bright field images, selective area diffraction patterns or high resolution lattice images were observed for image and structure analysis. The d space of diffraction planes were measured in a software (Digital Micrograph, Gatan).

2.2.4 Bonding strength (stud pull-out test)

A aluminum stud (head diameter 2.7 mm, length 12 mm, Quad Group, Spokane, WA, USA) was attached to the coating surface using a stainless steel clip (Quad Group, Spokane, WA, USA) and then glued under 150°C for 1 hour. The tensile bond strength of the MAO coating and titanium substrate was measured using a desktop universal mechanical tester (AG-IC, SHIMADZU co., Kyoto, Kyoutofu, Japan) under a cross head speed of 0.1 mm/min. Fifteen samples each groups were prepared for the stud pull-out test, the bonding strength was calculated and expressed using the equation below (1).

$$\text{Bonding strength (MPa)} = \frac{\text{Max. detached force (N)}}{\text{Area of the stud (mm}^2\text{)}} \quad (1)$$

Because the HA precipitates on the HT group peered off and the MAO layer was de-lamellar during the cleaning process (as show in Figure S1), we didn't performed the tensile bond strength on HT group.

2.2.5 Wettability

The hydrophilicity of the MAO surface was determined using a contact angle analyzer (FTA-125, First Ten Angstroms, Portsmouth, VA, USA). After a 10 μL droplet of distilled water (vertically extruded from a 31G needle) was suspended on the MAO titanium disc at room temperature, a continue record CCD was triggered and pictured. The contact angle of each water drop on the picture was measured automatically by a non-spherical fitting approach (Figure S2). Each reported contact angle is the mean of at least three independent measurements.

2.3 Biological evaluation

2.3.1 Protein adsorption

For fibronectin (Fn) adsorption test, the samples were immersed in 400 μl with 100μg/mL Human plasma fibronectin (Gibco #33016-015, Grand Island, NY, USA) and incubated in 24well plate for 6 h at 37°C. For bovine serum albumin (BSA) adsorption test, the samples were respectively immersed in BSA (2 mg/mL, Sigma) 400 μL/well for 2 h at 37°C in 24 well. After soaking for Fn or BSA, the samples were washed 3 times in PBS and detected by BCA protein assay kit (Pierce, Rockford, Ill, USA), and the wavelength was then measured at 570 nm by Versa Max ELISA microplate reader (Molecular Devices, CA, USA).

2.3.2 Cell culture

Human osteosarcoma cells (MG63 cells) were purchased from Bioresource Collection and Research Center (BCRC, Taiwan). The cells were grown in a minimum essential medium (α-MEM, Gibco, USA) containing nonessential amino acids and supplemented with 10% fetal bovine serum (FBS), 100mg/mL of streptomycin, 100 U/mL of penicillin. Cells were maintained in a humidified atmosphere with 5% CO_2 at 37°C. The culture medium was renewed twice per week. The MG63 cells of the tenth passage were detached using 0.25% trypsin in phosphate-buffered saline and resuspended in α-MEM until experimental use.

2.3.3 Cell morphology and cell spreading percentage

The cells were cultured on the titanium discs at 5×10^4 cells/disc for 4 hr. After that the samples were cleaned with PBS followed by 4% formaldehyde fixation, alcohol dehydration and critical point dried. Finally, the samples were fixed on a holder and coated with platinum. The initial cell adherent was observed by scanning electronic microscopy (JSM-6300, JEOL Ltd., Tokyo, Japan). The percentage of cells revealing spread morphology was quantified by dividing the number of spread cells by the total number of adherent cells. The spread cell is defined as the cell expends the lamellipodia to a double length of its original cell radius. Average percentages and standard deviations were calculated in five areas in 100 × pictures from two independent experiments.

2.3.4 Cell viability and alkaline phosphatase (ALP) activity

The test methods for observation of cell proliferation and the cell differentiation was described in previous paper [23, 24]. The cells were seeded at a density of 1×10^3 cells per disc (well) onto the titanium discs and incubated in a 24-well plate for 1, 7, and 14 days. Cell viability was evaluated using an enzymatic assay for mitochondria1 dehydrogenase activity, WST-8 [2-(2-methoxy-4-nitrophenyl)-3-(4-nitrophenyl)-5-(2,4-disulfophenyl)-2H-tetrazolium, monosodium salt] assay. WST-8 is reduced by dehydrogenases in cells to yield a yellow product (formazan), which is soluble in the tissue culture medium, and the amount of formazan generated by dehydrogenase activity in cells is directly proportional to the number of living cells. The optical density (OD) value of the dissolved solute was then measured by an ELISA reader (Versa Max, Molecular Devices, CA, USA) at a 450 nm wavelength. Measurements were performed in triplicate. Cell viability was calculated by the mean OD of three individual wells in the same group and expressed as normalized of control (MAO group). The total protein level and intracellular alkaline phosphatase (ALP) activity was examined at 1, 7, and 14 days. The attached MG63 cells in the 24-well plates reacted with 400 mL of cell lysis solution (500 mL TRIS-HCl, 1M stock solution, pH 7.4, 49.45 mL of distilled water, 50 mL TX-100 and $MgCl_2$ powder 2.38 mg) at 80°C for over 20 hr. Twenty-five microliter aliquots were transferred to a 96-well plate used to estimate alkaline phosphatase activity and total protein level. Total protein synthesis in the cell lysates was determined using a commercially available kit (BCA protein assay kit, Pierce Chemical Co., Rockford, Illinois, USA). Two hundred microliter of working reagent was added to each well for 30 min to incubate at 37°C. The absorbance was read using an ELISA reader at 562nm and was correlated to a standard protein curve. The amount of enzyme ALP of the lysed cells in the 96-well plate was quantified using a colorimetric assay with 200 mL of p-nitrophenylphosphate (Sigma) as substrate. After incubation at room temperature for 30 min, 25 mL of 3 M NaOH was added into the wells to stop color changing; the absorbance was determined at 405 nm. The values of ALP activity were normalized to the total protein obtained by BCA assay, and the values were expressed as nmol/μg protein. Triplicate samples from each group were analyzed.

2.4 Statistic evaluation

We analyzed data by overall one-way ANOVA followed by Tukey's test for individual between-group comparisons using a software (Origin 8.0, Microcal Software Inc., Northampton, MA, USA). The significant differences were set to $p<0.05$ if not specified.

3. Results

3.1. Characterzations of the surface coating

3.1.1. Morphology and Chemical composition

The microwave irradiation process significantly changes the surface morphology of MAO titanium surface. As shown in Figure 2, the pH and ions in the conditional mediums affect the shapes of the nano-scaled precipitates. The microwave irradiated MAO surfaces (Figure 2**a** ~ 2**f**) show a homogeneous porous surfaces, and the size and features of interconnected pores are not altered when compare to MAO control. The enlarged MAO surface (top right of Figure 2**a**) revealed a really flat feature under nano-scale. On other hand, whiskers and hexagonal columns (around 10 μm length, 5 μm diameter) crystalline precipitates (14.4 at% Ca, 10.3 at% P) are scattered on the HT conditioned MAO surface (Figure 2**b**). The MAO substrate of HT is fill with nano-scale surface precipitates (0.3 at% Ca, 1.1 at% P). The EDS area analysis (Table 1) shows the HT group has a lower overall Ca and P concentrations compare to microwave irradiated MAO and controlled MAO surfaces. The microwave irradiated MAO surfaces possess similar Ca and P concentration to the controlled MAO surface (5.8 at% Ca, 5.4 at% P), except that the MWCP11 show a slightly lower P concentration (3.9 at%). The enlarged pictures show numerous precipitates formed as pyramid spikes or nano-rod on the MWDD (Figure 2**c**) and MDCP (Figure 2**d**) surfaces. When increase the pH value of the condition medium (MWCP9 and MWCP11), the surface precipitates become to change their crystalline shape to cotton-like (Figure 2**e** and Figure 2**f**).

Table 1. The chemical concentration (in atomic percentage, at %) of samples by EDS analysis.

Elements, at%	MAO	HT	MWDD	MWCP	MWCP9	MWCP11
O	70.0	71.8	71.0	70.9	70.4	72.5
P	5.4	2.8 [1]	4.8	4.7	4.9	3.9
Ca	5.9	2.7 [1]	5.1	5.3	4.9	5.2
Ti	18.7	22.8	19.0	19.0	19.8	18.4

[1] The Ca and P concentration of substrate (0.3 at% Ca and 1.1 at% P) and crystalline phase (14.4 at% Ca and 10.3 at% P) on HT were detected using point analysis.

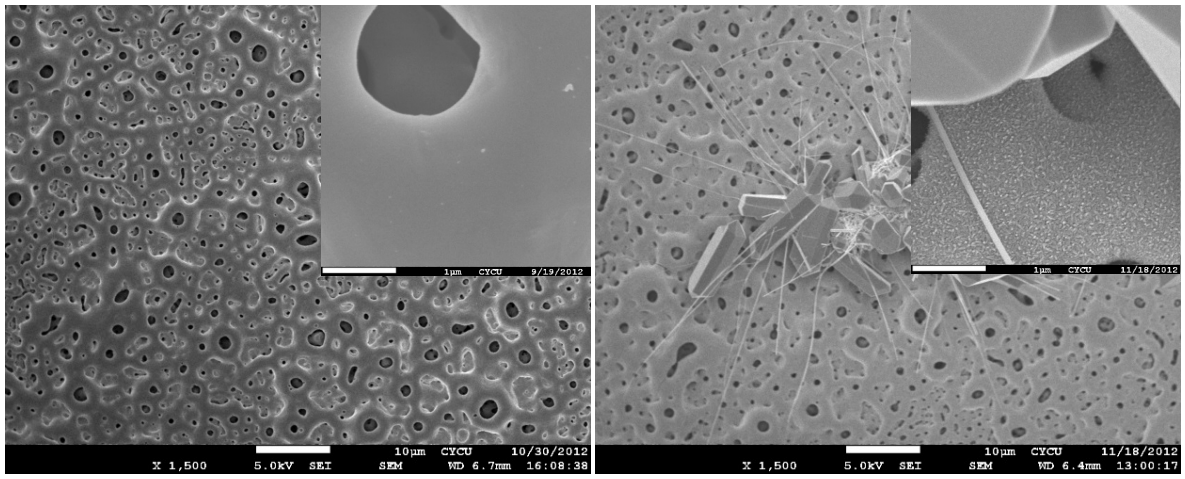

(**a**) (**b**)

(**c**) (**d**)

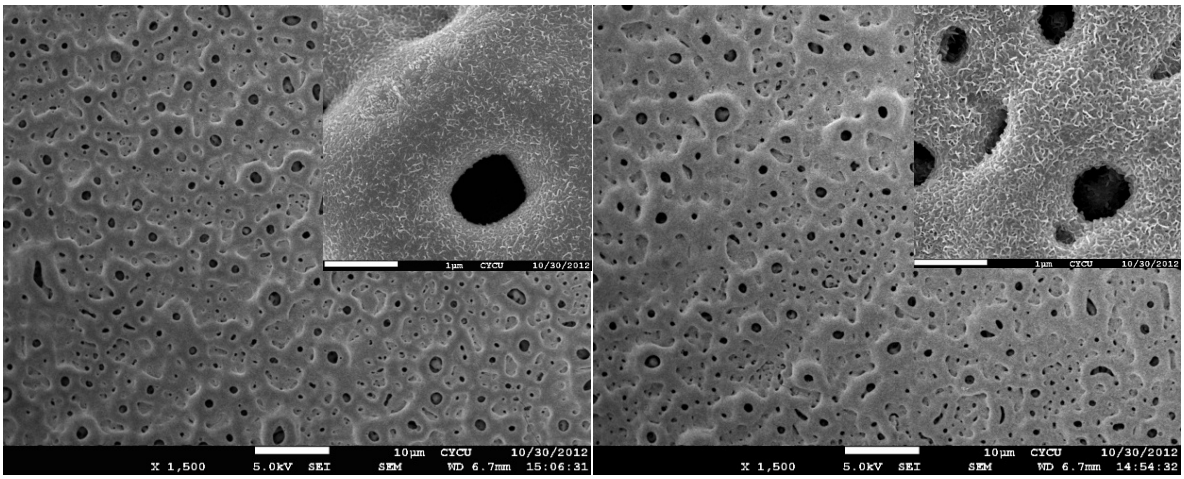

(**e**) (**f**)

Figure 2. The SEM surface morphologies of (**a**) MAO, (**b**) HT, (**c**) MWDD, (**d**) MWCP, (**e**) MWCP9, and (**f**) MWCP11. (1000x, left columns; 5000x, right columns)

3.1.2. Phase structures and bonding strength

The phase structures obtained by grazing angle XRD of the surface layer of MWDD, MWCP, MWCP9, MWCP11, and HT, are compared to the controlled MAO samples as shown in Figure 3**a**. The patterns demonstrate that the titanium oxides produced on the MAO surface at voltage of 280V are mainly possess anatase phase (reflection planes of (1 0 1) and (0 0 4) at 25.3° and 37.9°), which confirms to previous papers [9, 23, 25]. The reflection peaks at 31.7°, 32.2°, and 32.9° were assigned to the (2 1 1), (1 1 2) and (3 0 0) plane reflections of the hydroxyapatite (JCPDS#09-0432), which are only found in the traditional HT condition. Moreover the significant increasing intensity of anatase (1 0 1) reflection plane on HT indicated that the crystallinity of anatase on the MAO layer was increased after traditional hydrothermal process. The FTIR spectra of the coating layers are shown in Figure 3**b**. Two broaden IR resorption peaks around were recorded near 600 cm^{-1} and 1050 cm^{-1}. The strongest peak around 600 cm^{-1} was assigned to Ti-O (610 cm^{-1}) or Ti-O-Ti (475 cm^{-1}) bonds in anatase [26, 27]. While the broadened peak around 1050 cm^{-1} belong to the combination of P-O (PO_4^{3-}, 1006 cm^{-1}; HPO_4^{2-}, 1077/989 cm^{-1}; H_2PO^{4-}, 1155/1075 cm^{-1}) and P-OH (HPO_4^{2-}, 847 cm^{-1}; H_2PO^{4-}, 874 cm^{-1}) in the MAO layer [28] or P-O (PO_4^{3-}, 1011/632/602/565 cm^{-1}) in the HA crystals [29]. The mean bonding strength measured for the MWDD (51.1 ± 9.5 MPa), MWCP 38.2 ± 2.5 MPa), MWCP9 (30.1 ± 1.3 MPa), and MWCP11 (25.4 ± 5.5 MPa) samples were well above the minimum requirement of 22 MPa, which recommended by the regulator recognized standard ASTM F-1147 “Tension testing of calcium phosphate and metallic coatings”. However the MAO oxide layer becomes weakened by the traditional HT process, the coating peer off after the samples been sonicated in water for 30 minutes for clearing purpose (Supplement Figure **S**1).

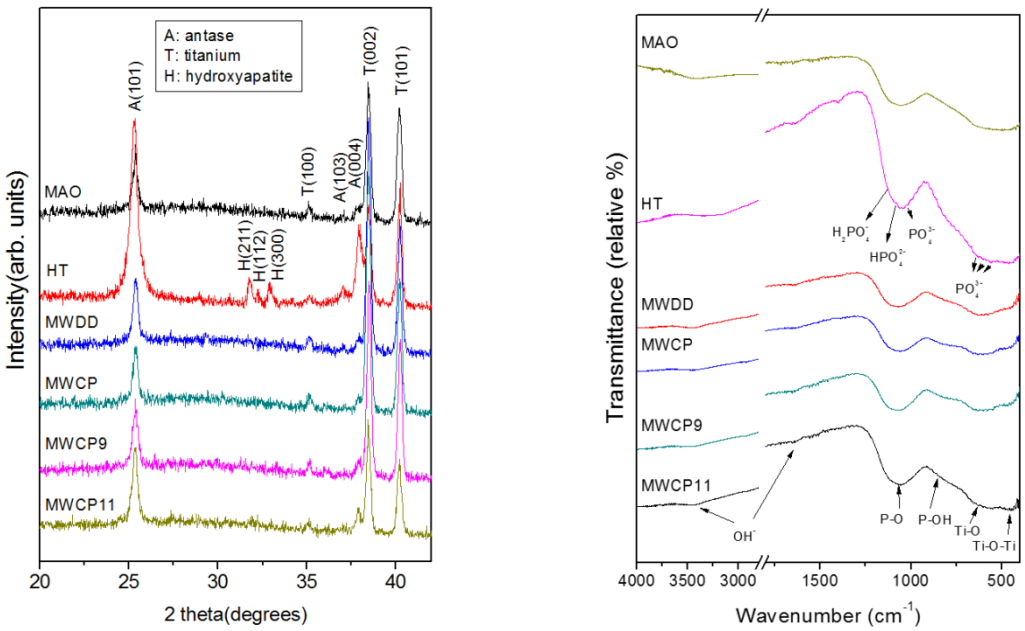

Figure 3. (**a**) X-ray deflection patterns and (**b**) FTIR spectra show the surface phase structures of microwave/hydrothermal treated MAO samples (MWDD, MWCP, MWCP9, MWCP11), hydrothermal treated MAO (HT), compare to the controlled MAO samples.

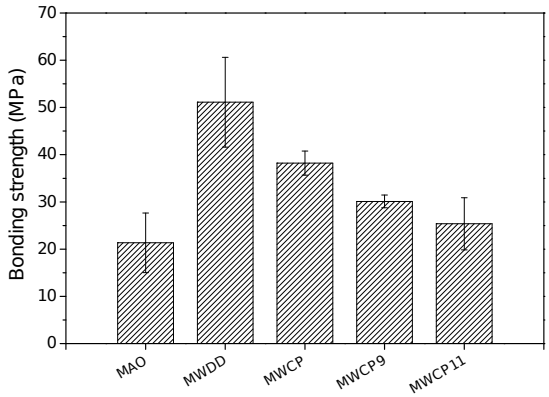

Figure 4. Bonding strength of the MAO coatings measured by a stud pull-out test. (n=15)

3.1.3. Transmission electron microscopy (TEM)

The morphology and structure of nano-scale precipitates investigated by TEM were shown in Figure 5. Nano-rod shape anatase precipitates were found in HT and MWCP groups (Figure 5**a**, 5**b** and Figure 5**g**, 5**h**). The nano-rod is 10-20 nm in diameter and 20-100 nm in length. The size of precipitates on MWDD surface is similar to MWCP but the shape is pyramid-like (Figure 5**d**, 5**e**). Similar SAED patterns were observed on precipitates of HT, MWDD, and MWCP groups, the scattering ring pattern (Figure 5**c**) demonstrated that nano-crystals are TiO_2 anatase structure. By high resolution lattice images, apparently the nano-rod or nano-pyramid anatase were all precipitated along the {0 0 1} direction. The surface of nano-rod anatase crystals on HT group parallel to {1 0 0} face (Figure 5**b**), while the nano-pyramid anatase crystals on MWDD and MWCP reveal zigzag surfaces predominated with anatase {1 0 1} faces (Figure 5**f**, 5**i**). An angle of 68.3° was found between {0 0 1} and {1 0 1} facets of anatase as shown in Figure 5**f** and 5**i**. The small picture at the corner of Figure 5**f** is a FFC reconstructed diffraction pattern of the lattice image, the pattern fits to the diffraction pattern of anatase (1 0 0) zone axis, which again confirmed the anatase crystalline structure. The MAO surfaces on MWCP9 and MWCP11 are randomly overlapped of nano-sheet precipitates (Figure 5**k**, 5**n**), as shown in the high resolution lattice image these nano-sheets contained dominant amorphous phase and some short range order area as marked by dash circles (Figure 5**l**). The SAED pattern of these nano-sheets shown heavily diffuse rings also

confirmed the loss of crystallinity as shown in Figure 5**o**. The EDS analysis demonstrated precipitates on the HT group has a relative lower Ca, P concentration (Ca: 2.2 at%, P: 4.9 at%) compare to that of MWDD (10.5 at%, 9.6 at%), MWCP (15.4 at%, 7.1 at%), MWCP9 (12.8 at%, 5.3 at%), and MWCP11(17.8 at%, 6.2 at%). And the Ca concentration of the precipitates is increased with increased pH values of the conditioned solutions in microwave process.

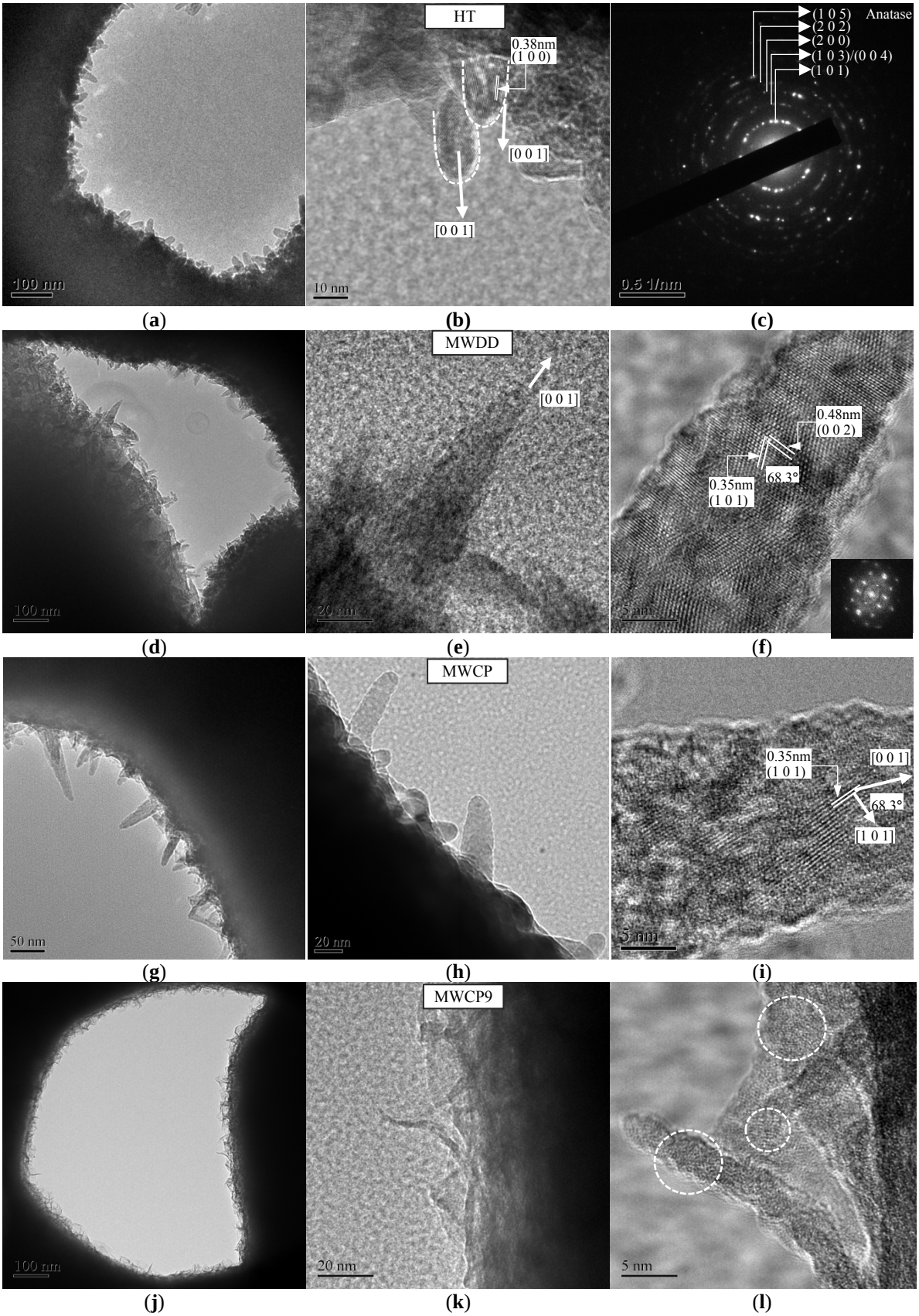

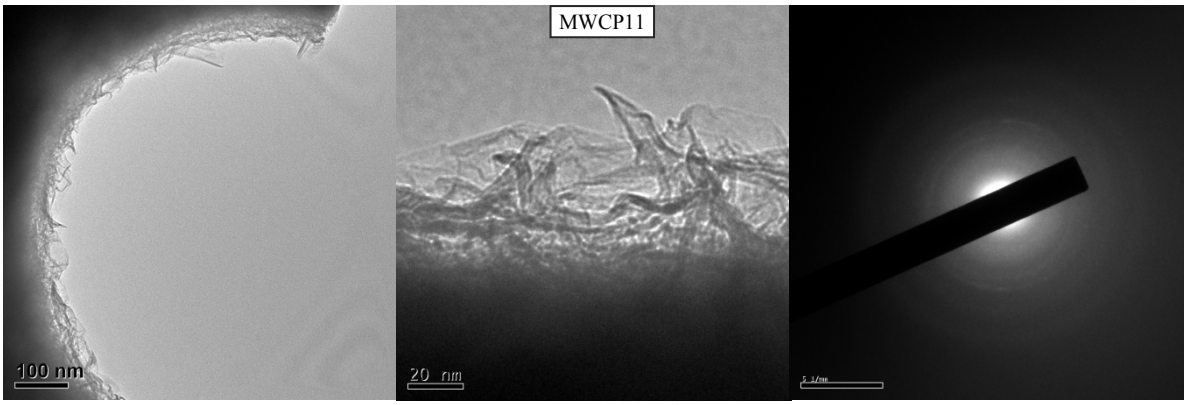

(**m**) (**n**) (**o**)

Figure 5. TEM investigation (BF, SAED, high resolution image) of nano precipitates on the MAO titanium surface after hydrothermal and microwave irradiation process. (**a**)~(**c**) HT, (**d**)~(f) MWDD, (g)~(i) MWCP, (j)~(l) MWCP9, (m)~(o) MWCP11.

3.1.4. Hydrophilicity (wettability)

As shown in Figure 6, superior hydrophilicity are obtained in the MW groups in which the contact angles are equal to or below 10° and are much lower than that of MAO (84.9 ± 0.5°). The contact angle of HT (38.5 ±1.5°) is much lower than that of MAO, but is still higher than that of MW groups. Obviously the microwave-irradiated modification to the MAO titanium improving the wettability of MAO titanium. The contact angle of MWDD (8.3 ± 1.4°) and MWCP (7.2 ± 0.5°) were significantly lower than MAO, but higher than that of MAO. The contact angle of MWCP9 (5.6 ±0.3°) is similar to that of MWCP11 (5.3 ± 1.5°).

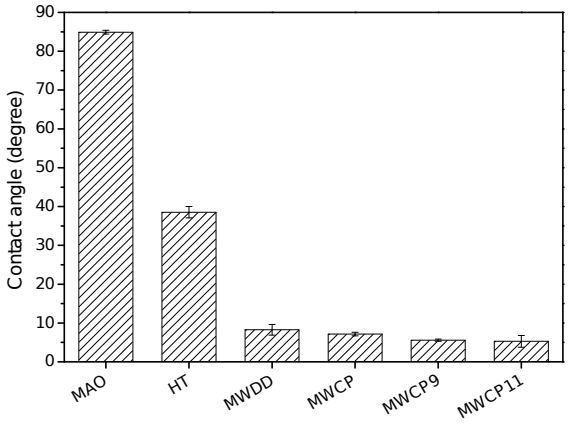

Figure 6. Hydrophilicity (wettability) of MAO, HT, MWDD, MWCP, MWCP9, and MWCP11 titanium discs were measured by water contact angle. The MWDD, MWCP, MWCP9, and MWCP11 groups show a super-hydrophilicity feature (contact angle below 10°).

3.2. In-vitro biological evaluations

3.2.1. Protein adsorption

Figure 7 shows quantitative analysis of fibronectin (Fn) and bovine serum albumin (BSA) adsorptions of MW processed MAO titanium compared to MAO and HT groups. The amounts of fibronectin adsorbed on the HT, MWDD, MWCP, MWCP9, and MWCP11 were significantly higher than that of MAO group after incubated for 6 hr (* in Figure 7**a**, $p < 0.01$). The adsorption of BSA among groups also present significant different, where the amounts of BSA adsorbed on the HT, MWDD, MWCP, MWCP9, and MWCP11 were significantly higher than that of MAO group (* in Figure 7**b**, $p < 0.01$), and the MWCP11 was found significantly higher than that of HT group (** in Figure 7**b**, $p < 0.05$).

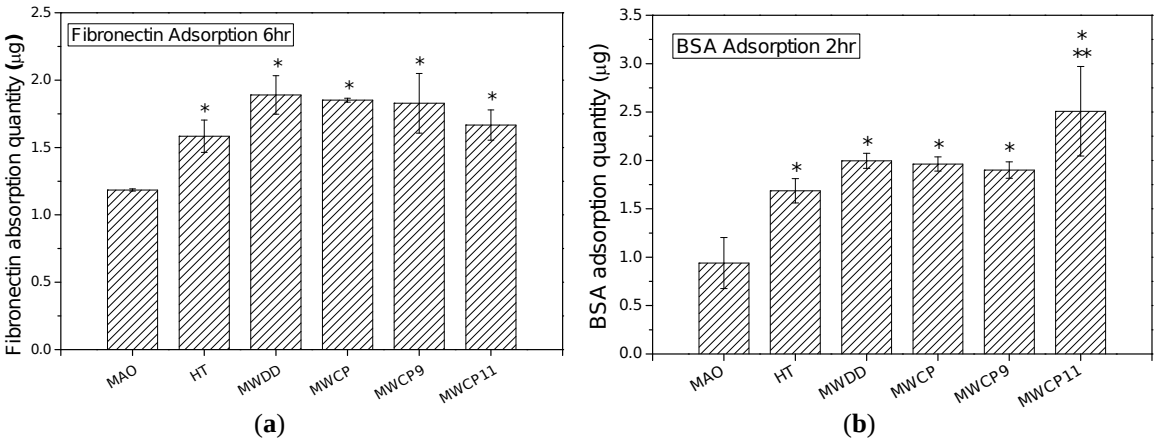

Figure 7. Quantitative analysis of proteins adsorption on the samples. **(a)** Fibronectin and **(b)** bovine serum albumin (BSA) adsorption on surfaces of MAO, HT, MWDD, MWCP, MWCP9, and MWCP11. Samples were immersed in fibronectin and bovine serum albumin for 6 hr and 2 hr respectively.

3.2.2. Cells initial attachment and spreading

The cells revealed more flatten than that on the HT and MAO surface after culture for 4 hr (Figure 8). The enlarged pictures (right column in Figure 8) shows the extension of lamellipodia and the spreading of filopodia of MG63 cells was prone to the MW groups, on the contrary, the cells were maintain hemispherical on the MAO surface (Figure 8**a**, 8**d**) or enclasp firmly to the HA crystals on the HT surface (Figure 8**c**, 8**d**). The MAO surface without nano-feature also present less affinity to the initial cell adherent. The spreading rate of the cells were quantified in Table S1. The MW groups present higher spreading percentage than that of HT and MAO groups. And the total cell numbers (counting by five SEM 100x pictures) of HT is lower than other groups.

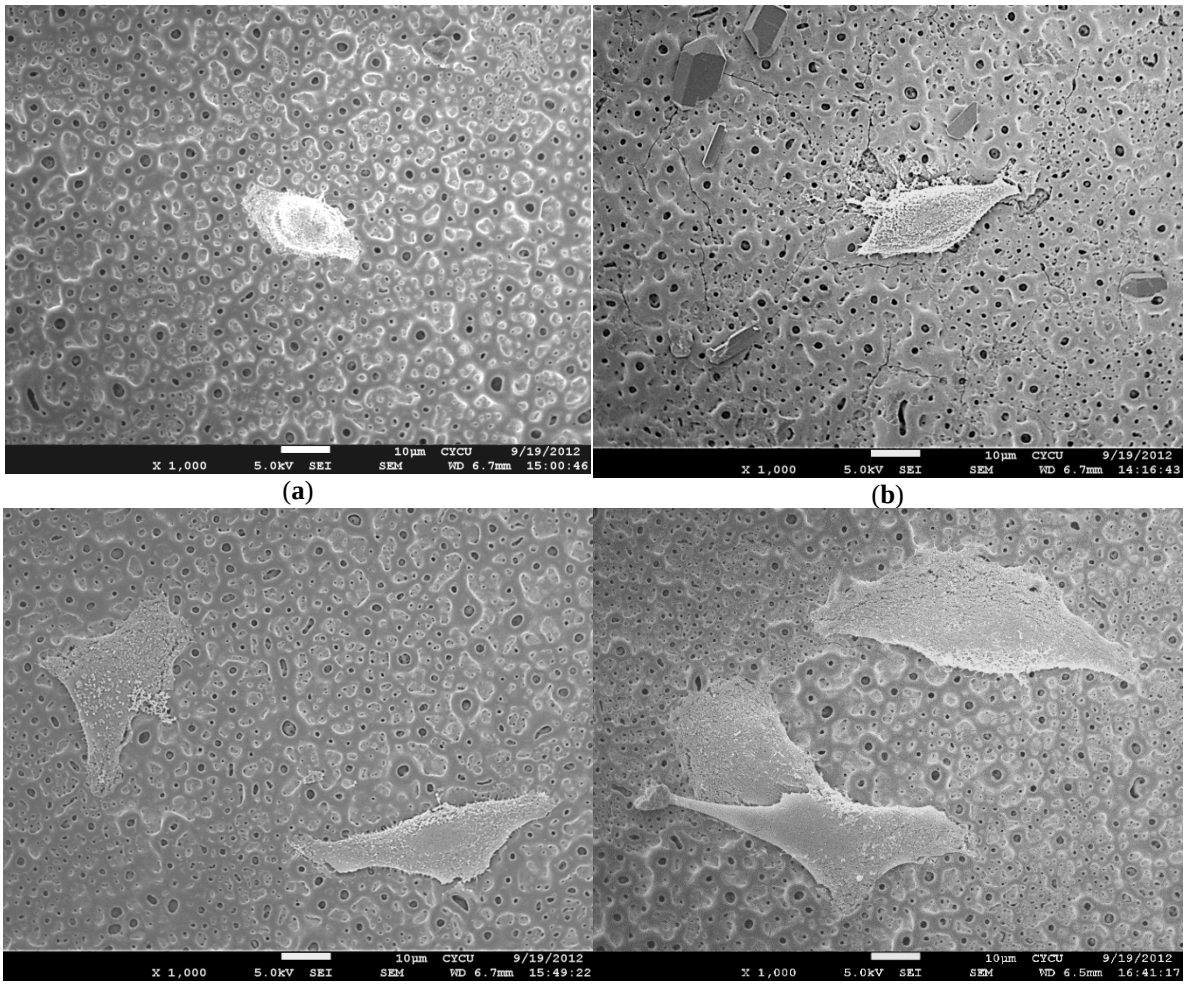

(**c**) (d)

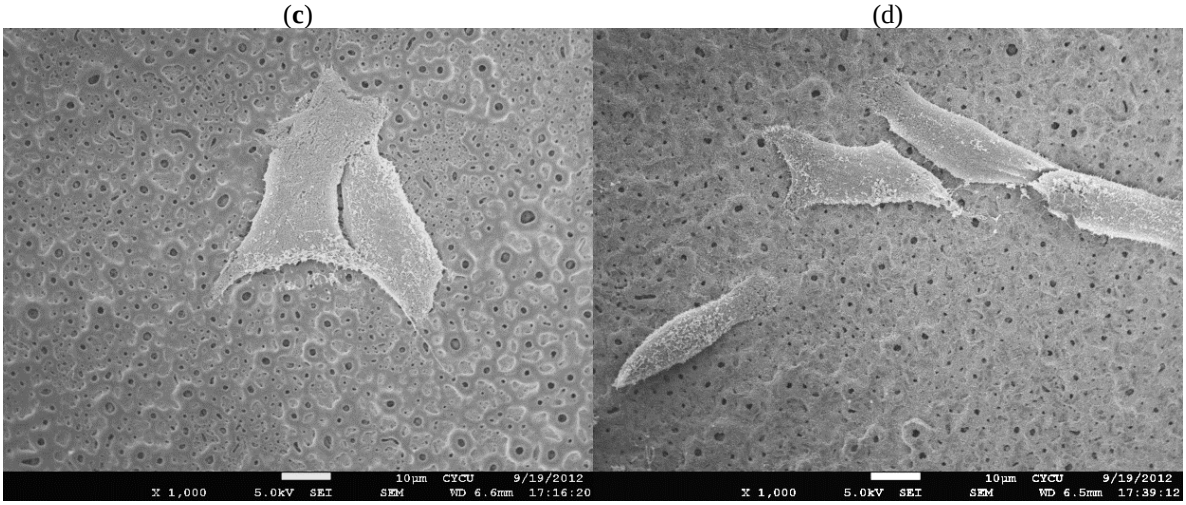

(**e**) (**f**)

Figure 8. The SEM morphologies of MG63 cells attachment (4 hr) on (**a**) MAO, (**b**) HT, (**c**) MWDD, (**d**) MWCP, (**e**) MWCP9, and (**f**) MWCP11.

3.2.3. Cell proliferation (WST assay) and differentiation activity (ALP assay)

The results of cell viability and differentiation ability of MG63 cultured on different conditioned titanium discs were shown in Figure 9. The proliferation was assessed using WST-8 assay (Figure 8**a**). The cell viability at the 1st day were similar in the MW groups, HT group, and MAO groups. At the 7th day, the MW groups (MWDD, MWCP, MWCP9, MWCP11) present higher cell viability than HT group and MAO group ($p < 0.05$). At the 14th day, the cell viability of MWCP11 were the similar to the MAO group, and significant higher than that of MWDD, MWCP9, and HT groups ($p < 0.05$).

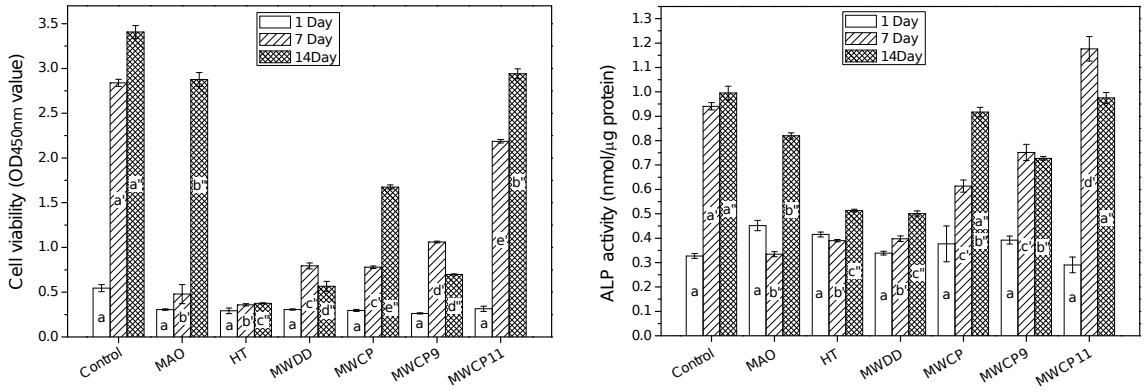

(**a**) (**b**)

Figure 9. (**a**) The cell viability (WST assay) and (**b**) alkaline phosphate activity (ALP assay) of MAO, HT, MWDD, MWCP, MWCP9, and MWCP11 with compared to the blank control (polystyrene, 24 well, well diameter 15.6 mm). The same letters marked in the columns present the same static level at the same time period.

The results of the alkaline phosphatase activity assay were present in Figure 9**b**. The data shows ALP activities of all groups at the 1st day are in the same level. At the 7th day, the MWCP, MWCP9, and MWCP11 groups present higher ALP activity than MAO, HT, and MWDD groups ($p < 0.05$). The MWCP11 group possesses highest ALP activity at the 7th and 14th day. The ALP activity of MWCP and MWCP9 were similar to the MAO groups at the 14th day.

4. Discussion

The MAO process is a commonly used technique to alter titanium dental implant surface topography having sub-micro to micro-scale roughness and interconnected pores [23] which are beneficial to the initial stability and osseo-integration of the dental implant. Nowadays implant surface with nano-scale topographies

have been proven play implant roles in the differentiation and destiny of adhered stem cells. However, very few study presents successful nano-scale modification to MAO surface. In this study, we demonstrated that the topography of MAO layer can be manipulated forming nano-pyramid, nano-rod shape anatase crystals, or 3D nano-sheet architecture amorphous anatase on the MAO surface by a very rapid and simple microwave process. It is expected that the microwave-irradiated MAO samples have higher population of nuclei with smaller size than the samples nucleated by conventional hydrothermal (HT). Although the HA crystals precipitate on the hydrothermal treated MAO had been studied previous [11, 13, 30-32], the formation of nano crystalline anatase has not been investigated. In the present study, two types of crystals are identified in HT group (250°C for 3 h); hexagonal HA crystals in micrometer scale (Figure 2**b**) and nano-rod anatase crystals (Figure 5**b**) which have 10 nm to 20 nm in diameter and 20 nm to 100 nm in length. The diameter of anatase nano-crysals in MWDD and MWCP groups are a little larger than that in HT group. However, the crystallinity of anatase on the MAO surface was increased by HT process (Figure 3**a**), which has not been mentioned in previous papers [9, 11, 13]. In addition, the Ca and P concentration on the anatase precipitates in HT (not the large HA crystal) are obviously lower than in the MW groups (Table 1). This difference may because that traditional HT process takes more time at hydrothermal condition, thus Ca and P ions in the amorphous region of MAO layer [9] have enough time to diffuse to the medium, as a result rapid growth of high crystallinity HA associate with high crystallinity nano-crystal anatase (containing less Ca, P ions) precipitated on the MAO surface. On the contrary, the high resolution lattice images of MWDD and MWCP demonstrated that sub-grains and amorphous zones were scattered throughout the anatase crystals (Figure 5**f** and 5**i)**, in which were distinguish from that in HT groups. On the other hand, the growth direction of anatase in MWDD and MWCP were happened to be the same as in HT group (Figure 5**b**), which means the anatase crystals precipitated with a prefer orientation under hydrothermal condition and microwave irradiation. It has been reported that under hydrothermal condition rapid growth occurs along [0 0 1] for pure TiO_2 anatase, driven in part by the relatively high surface energy of (0 0 1) and in part by a kinetic effect involving a cyclic generation of highly reactive adsorption sites [33].

In this study, the anatase in MWDD and MWCP groups present zigzag {1 0 1} pyramidal faces should be a result of that the microwave irradiation only process in a very short time (1 minute), thus the atoms do not have enough time to diffuse forming a flatten pyramidal faces [34]. The morphology of nano TiO_2 anatase is also controlled by the surface chemistry (hydrogen ions), thus the shape of nano anatase can be predict by altered the pH value [29]. The pyramid shape is a typical morphology of anatase crystal which was formed in neutral and acid environment. And it is suspected that the higher pH value of the conditioned solution tend to alter the charges on the surface thus hinder the crystallization of anatase [29]. As shown in the SAED pattern (HT, Figure 5**c**), the scattering spots on rings were well fit to the reflection planes of poly-crystalline anatase nano-precipitates, the same pattern were also found on the MWDD and MWCP. On the other hand, the MWCP11 surface showed a diffused ring pattern (Figure 5o), which indicates that the precipitates on the MAO is amorphous. Although the morphologies are different on the surfaces of microwave irradiated MAO, the main XRD reflection peaks (containing titanium and anatase crystal structure) on the surfaces of MWDD, MWCP, MWCP9, and MWCP11 were not significant changed from the MAO diffraction patterns (Figure 3**a**). Moreover, the chemical compositions of the MW samples were similar by EDS/SEM. Since the XRD and EDS/SEM detected the surface layer by tens to hundreds micrometer, the results confirm that the MW modification is only by nano-scale on the MAO layer and the MAO substrates under the modified layer were not change too much. The broaden IR peak around 600 cm^{-1} seems more prone to divided into two peaks (Ti-O and Ti-O-Ti) after the MAO discs been microwave irradiated, implies the crystallinity of the substrates might also be slightly increased after the microwave-assisted hydrothermal process (Figure 3**b**). The microwave derived nano-scale precipitates are not just formed on the surface, instead they were also found inside the inner pores of the MAO titania layer (Figure 2). That can be a merit to reduce the wear when the implant were forced in (or screwed in) the bone tissues. In addition, the nano-scale precipitates could adsorb more extracellular matrix (ECM) by the increased surface area and would provide sustained bioactivity in physical environment.

Although the increasing crystallinity of anatase on the surface of HT group was confirmed by XRD and FTIR, the bonding strength HT processed sample was fail to be measured while the coating peer off after the samples been sonicated in water for 30 minutes for clearing purpose (Figure S1). On the contrary, the temperature rise homogeneously under the microwave-assisted hydrothermal process and water in a very short time, thus the damage to the oxides/metal interface could be limited. A shown in Figure 4, the bonding strength of MWDD and MWCP even increased when compared to the original MAO coating. The increment of strength may because of that the increased surface energy are expected to improve the wettability of the bonding

adherent. But the bonding strength of MWCP11 is similar to that of MAO, which implies that the amorphous precipitate may be intrinsically weak and did not improve the adhesion.

The hydrophilicity (wettability) of implants largely inference the biological response and play an important role in the osteointegration [35]. Wettability is modulated by chemistry and topography of the extremely surface, and the result in changing the surface energy. As shown in Figure 6, the contact angle of MW groups all possess superior hydrophilicity (below 10°), indicate that the microwave-irradiated modification to the MAO titanium improving the wettability of MAO titanium (an original contact angle of 84.9 ± 0.49°). The hydrophilicity of the surface is crucial to the adsorbing proteins. It has been suggest that plasma fibronectin binds more to hydrophilic surfaces [20], whereas albumin binds more to hydrophobic surfaces [21]. However, the protein adsorption to surface is not only relative to the hydrophilicity, in this study the surfaces all possess hydrophilic surfaces, thus the "size effect" seem to dominate the protein adsorption. The MW surfaces (MWDD, MWCP, MWCP9, and MWCP11) all possess nano-scale and micro-to-submicron scale roughness, which are expected to provide more binding sites to adsorb proteins. As a result the Fn and BSA adsorptions were significant higher in these groups when compared to the MAO group (Figure 7**a** and 7**b**). The protein adsorption to surface is not only relative to the hydrophilicity but also to the crystal structure of titanium surfaces [21], chemistry and physical properties, such as surface area and charge [22, 36].

Fibronectin is a large extracellular glycoprotein with molecular weight around 440kDa. Unfolded fibronectin is 140 nm in length and 2 nm in diameter, and is more compact in near-physiological environment [37, 38]. On the contrary, BSA is in ellipsoid shape with a much smaller size of 140 × 40 × 40 Å [39]. In the present study, the MW groups all possess super hydrophilicity and similar roughness in micro-scale. The adsorption of fibronectin are similar among MW groups, which seems to regard to its larger size. On the other hand, it is noticeable that the MWCP11 group has a significantly higher BSA absorption than other groups (Figure 7**b**), which implied that a 3D nano-sheet architecture feature on the MWCP11 may provide more nano-scale (and sub-nano) heterogeneous binding sites to the BSA which has a smaller size than fibronectin. Albumin, the most abundant protein in blood likely to bind to the implant and has been extensively studied [22, 36]. The titanium oxide layer may has less attractive to the negatively charged (or have negatively charged groups) BSA when compared to that of the histone (positively charged), however, it can still bind to nanostructured TiO_2 surface by a mechanical interlock mechanism [22]. The nano-featured surface is believed to regulate cell behaver by adsorb proteins heterogeneously as functional ECM [5, 6], and stimulate the cell functions by mechanotransduction signaling pathways [6]. The titanium oxide layers contained divalent ions (especially calcium ion) are expected to binding more serum albumin and would improve to viability of MG63 cells [40]. The present results show that MW modified nano topography while maintaining Ca, and P ions in the MAO substrate, would enhance more MG63 cells adherent on the surface. Moreover, the higher calcium contents (only detected by EDS/TEM) on the nano-scale surface did not cause any cytotoxicity on the present groups.

Several studies addressed an aging effect of the wettability properties of titania nanotube surfaces fabricated by anodization, where the surface became more hydrophobic when aged in air over a period of time [41-43]. Using oxygen plasma treatment on nanostructured titanium oxide (TiO2) surfaces [44], the study show that osteoblast-like cell response could be enhanced by removed hydrocarbon contamination and removed fluorine impurities, which were present due to the electrochemical anodization process, even there is no differences in wettability between untreated and plasma treated surfaces. The paper suggested the hydrocarbon contamination and impurities may influence the cell affinity, but the microwave-assisted hydrothermal process was performed in DD or low concentration Ca/P solutions which are cleaned processes. And the carbon content on the surface are detected as the same level. Moreover, the MAO process involved a higher applied voltage, usually above 150V (280V in the present study), which was much higher than that of nano-tube anodization of about 10 Volts and the hydrocarbon contamination would eliminated under plasma condition. We will further studies on the surface potential, nano-roughness (AFM) and electron spectroscopy for chemical analysis (ESCA) structure refining to clarify the detail nucleation mechanism of nano-scale precipitates under microwave-assisted hydrothermal process with regard to their biological interaction.

The anatase formed on the MAO surface change their shape may alter the charge density, and thus accumulate a higher electron density to the pyramid sharp edges, these negative charges on the anatase crystal planes will promote the adhesion of osteoblasts [45]. Nano-to-submicron scale surface has been proved to enhance osteoblast proliferation, differentiation [3, 42], and ultimately induced higher expression of osteoblast phenotype genes [5]. However, a recently paper using hydrothermal method to create nano-scale feature on MAO titanium surface fail to demonstrate biological affinity. They explain the nano-topology should more important than the hydrophilicity of the coating [14]. However the chemical composition and crystallinity of

their nano-topology layer is unknown. In our study, the nano-pyramid and nano-rod anatase (MWDD and MWCP) and 3D nano-sheet amorphous anatase (MWCP9 and MWCP11) were formed on the MAO surface with super hydrophilicity and enhanced protein adsorption of the MAO surface. The higher BSA adsorption rate on MWCP11 is due to the possible increasing sub-nano binding sites in the 3D nano-sheet architecture. Although the environment around implant surface will become more complex in vivo, the present in-vitro study demonstrates that the microwave process would be an effective method to produce a controlled nano-topography without compromise the bonding strength. The MW modified nano feature surface can be expected to adsorb more ECM in vivo and conduct the osteoblasts cell adherent, enhancing cell proliferation, and cell differentiation thus facilitate osseointegration.

5. Conclusions

We introduce a simple route to produce nano-topography on the MAO titanium surface, which is super-hydrophilic, high affinity for proteins can promote cell attachment and cell differentiation. The MW process shorten the traditional HT processing time and the MAO surface has been modified in its nano-topography without compromise the bonding strength. The MWDD featured with nano-pyramid anatase crystals and the MWCP11 surface precipitates with 3D nano-sheet architecture amorphous anatase which present higher biological affinity. The microwave irradiation process is a rapid, simple and controllable method that could be a suitable process for producing nano-scale topographies on MAO titanium for implant applications.

Supplementary Materials: The following are available online at www.mdpi.com/link, Figure S1: The morphology of HT sample before (a) and after (b) the sonicated clean in DD water for 30 minutes. The HA precipitates peered off and the MAO layer was de-lamellar (red arrows) during the cleaning process, Table S1: Adherent cell number and spreading percentage of MG63 cells on the samples after cultured for 4 hr.

Acknowledgments: This work was supported by grants from the National Science Council, Taiwan, R.O.C. (NSC 101-2320-B-039-004-MY3; MOST 105-2314-B-039-046-MY2).

Author Contributions: **D**.J. Lin conceived and designed the experiments; **D**.J. Lin, C.Y. Chen, and W.C. Chen performed the experiments; **D**.J. Lin analyzed the data; J.H. Chern Lin and C.C. Chen contributed reagents/materials/analysis tools; **D**.J. Lin and L.J. Fuh wrote the paper.

Conflicts of Interest: The authors declare no conflict of interest.

References

[1] M.M. Shalabi, A. Gortemaker, M.A. Van't Hof, J.A. Jansen, N.H. Creugers, Implant surface roughness and bone healing: a systematic review, J Dent Res, 85 (2006) 496-500.

[2] M. Goldman, G. Juodzbalys, V. Vilkinis, Titanium surfaces with nanostructures influence on osteoblasts proliferation: a systematic review, J Oral Maxillofac Res, 5 (2014) e1.

[3] G. Zhao, O. Zinger, Z. Schwartz, M. Wieland, D. Landolt, B.D. Boyan, Osteoblast-like cells are sensitive to submicron-scale surface structure, Clin Oral Implants Res, 17 (2006) 258-264.

[4] R.A. Gittens, T. McLachlan, R. Olivares-Navarrete, Y. Cai, S. Berner, R. Tannenbaum, Z. Schwartz, K.H. Sandhage, B.D. Boyan, The effects of combined micron-/submicron-scale surface roughness and nanoscale features on cell proliferation and differentiation, Biomaterials, 32 (2011) 3395-3403.

[5] D. Khang, J. Choi, Y.M. Im, Y.J. Kim, J.H. Jang, S.S. Kang, T.H. Nam, J. Song, J.W. Park, Role of subnano-, nano- and submicron-surface features on osteoblast differentiation of bone marrow mesenchymal stem cells, Biomaterials, 33 (2012) 5997-6007.

[6] P.M. Tsimbouri, Adult Stem Cell Responses to Nanostimuli, J Funct Biomater, 6 (2015) 598-622.

[7] N. Hori, F. Iwasa, T. Ueno, K. Takeuchi, N. Tsukimura, M. Yamada, M. Hattori, A. Yamamoto, T. Ogawa, Selective cell affinity of biomimetic micro-nano-hybrid structured TiO2 overcomes the biological dilemma of osteoblasts, Dent Mater, 26 (2010) 275-287.

[8] Q.B. Li, W.B. Yang, C.C. Liu, D.A. Wang, J. Liang, Correlations between the growth mechanism and properties of micro-arc oxidation coatings on titanium alloy: Effects of electrolytes, Surface & Coatings Technology, 316 (2017) 162-170.
[9] C.S. Lin, M.T. Chen, J.H. Liu, Structural evolution and adhesion of titanium oxide film containing phosphorus and calcium on titanium by anodic oxidation, Journal of Biomedical Materials Research Part A, 85A (2008) 378-387.
[10] D.Q. Wei, Y. Zhou, C.H. Yang, Structure, cell response and biomimetic apatite induction of gradient TiO2-based/nano-scale hydrophilic amorphous titanium oxide containing Ca composite coatings before and after crystallization, Colloids and Surfaces B-Biointerfaces, 74 (2009) 230-237.
[11] H. Ishizawa, M. Ogino, Thin hydroxyapatite layers formed on porous titanium using electrochemical and hydrothermal reaction, Journal of Materials Science, 31 (1996) 6279-6284.
[12] F. Liu, Y. Song, F. Wang, T. Shimizu, K. Igarashi, L. Zhao, Formation characterization of hydroxyapatite on titanium by microarc oxidation and hydrothermal treatment, Journal of Bioscience and Bioengineering, 100 (2005) 100-104.
[13] X. Zhu, D.W. Son, J.L. Ong, K. Kim, Characterization of hydrothermally treated anodic oxides containing Ca and P on titanium, J Mater Sci Mater Med, 14 (2003) 629-634.
[14] Y.H. Song, J.H. An, Y.W. Seo, W.J. Moon, Y.J. Park, H.J. Song, Osteoblast cell adhesion and viability on nanostructured surfaces of porous titanium oxide layer, J Nanosci Nanotechnol, 14 (2014) 5682-5687.
[15] Y.D. Li, W.Q. Wang, J.T. Duan, M. Qi, A super-hydrophilic coating with a macro/micro/nano triple hierarchical structure on titanium by two-step micro-arc oxidation treatment for biomedical applications, Surface & Coatings Technology, 311 (2017) 1-9.
[16] S.H. Jhung, T.H. Jin, Y.K. Hwang, J.S. Chang, Microwave effect in the fast synthesis of microporous materials: Which stage between nucleation and crystal growth is accelerated by microwave irradiation?, Chemistry-a European Journal, 13 (2007) 4410-4417.
[17] K.J. Rao, B. Vaidhyanathan, M. Ganguli, P.A. Ramakrishnan, Synthesis of inorganic solids using microwaves, Chem Mater, 11 (1999) 882-895.
[18] T.S.S. Kumar, I. Manjubala, J. Gunasekaran, Synthesis of carbonated calcium phosphate ceramics using microwave irradiation, Biomaterials, 21 (2000) 1623-1629.
[19] S. Sarig, F. Kahana, Rapid formation of nanocrystalline apatite, J Cryst Growth, 237 (2002) 55-59.
[20] D.E. MacDonald, N. Deo, B. Markovic, M. Stranick, P. Somasundaran, Adsorption and dissolution behavior of human plasma fibronectin on thermally and chemically modified titanium dioxide particles, Biomaterials, 23 (2002) 1269-1279.
[21] R. Jimbo, M. Ivarsson, A. Koskela, Y.T. Sul, C.B. Johansson, Protein adsorption to surface chemistry and crystal structure modification of titanium surfaces, J Oral Maxillofac Res, 1 (2010) e3.
[22] M. Kulkarni, A. Mazare, J. Park, E. Gongadze, M.S. Killian, S. Kralj, K. von der Mark, A. Iglic, P. Schmuki, Protein interactions with layers of TiO2 nanotube and nanopore arrays: Morphology and surface charge influence, Acta Biomaterialia, 45 (2016) 357-366.

[23] D.-J. Lin, M.-T. Tsai, T.-M. Shieh, H.-L. Huang, J.-T. Hsu, Y.-C. Ko, L.-J. Fuh, In vitro antibacterial activity and cytocompatibility of bismuth doped micro-arc oxidized titanium, Journal of Biomaterials Applications, 27 (2013) 553-563.
[24] L.J. Fuh, Y.J. Huang, W.C. Chen, D.J. Lin, Preparation of micro-porous bioceramic containing silicon-substituted hydroxyapatite and beta-tricalcium phosphate, Materials Science & Engineering C-Materials for Biological Applications, 75 (2017) 798-806.
[25] M. Rico-Santacruz, A.E. Sepulveda, E. Serrano, E. Lalinde, J.R. Berenguer, J. Garcia-Martinez, Organotitanias: a versatile approach for band gap reduction in titania based materials, Journal of Materials Chemistry C, 2 (2014) 9497-9504.
[26] W.Q. Gong, A real time in situ ATR-FTIR spectroscopic study of linear phosphate adsorption on titania surfaces, International Journal of Mineral Processing, 63 (2001) 147-165.
[27] M. Nakamura, D. Korzec, T. Aoki, J. Engemann, Y. Hatanaka, Characterization of TiOx film prepared by plasma enhanced chemical vapor deposition using a multi-jet hollow cathode plasma source, Applied Surface Science, 175-176 (2001) 697-702.
[28] O. Albayrak, M. Ipekoglu, N. Mahmutyazicioglu, M. Varmis, E. Kaya, S. Altintas, Preparation and characterization of porous hydroxyapatite pellets: Effects of calcination and sintering on the porous structure and mechanical properties, Proceedings of the Institution of Mechanical Engineers Part L-Journal of Materials-Design and Applications, 230 (2016) 985-993.
[29] A.S. Barnard, L.A. Curtiss, Prediction of TiO2 nanoparticle phase and shape transitions controlled by surface chemistry, Nano Lett, 5 (2005) 1261-1266.
[30] F. Liu, Y. Song, F.P. Wang, T. Shimizu, K. Igarashi, L.C. Zhao, Formation characterization of hydroxyapatite on titanium by microarc oxidation and hydrothermal treatment, Journal of Bioscience and Bioengineering, 100 (2005) 100-104.
[31] A. Kossenko, S. Lugovskoy, N. Astashina, A. Lugovskoy, M. Zinigrad, Effect of time on the formation of hydroxyapatite in PEO process with hydrothermal treatment of the Ti-6Al-4V alloy, Glass Physics and Chemistry, 39 (2013) 639-642.
[32] A. Lugovskoy, S. Lugovskoy, Production of hydroxyapatite layers on the plasma electrolytically oxidized surface of titanium alloys, Materials Science & Engineering C-Materials for Biological Applications, 43 (2014) 527-532.
[33] R.L. Penn, J.F. Banfield, Morphology development and crystal growth in nanocrystalline aggregates under hydrothermal conditions: insights from titania, Geochimica Et Cosmochimica Acta, 63 (1999) 1549-1557.
[34] C.H. Cho, M.H. Han, D.H. Kim, D.K. Kim, Morphology evolution of anatase TiO2 nanocrystals under a hydrothermal condition (pH=9.5) and their ultra-high photo-catalytic activity, Materials Chemistry and Physics, 92 (2005) 104-111.
[35] F. Rupp, R.A. Gittens, L. Scheideler, A. Marmur, B.D. Boyan, Z. Schwartz, J. Geis-Gerstorfer, A review on the wettability of dental implant surfaces I: Theoretical and experimental aspects, Acta Biomaterialia, 10 (2014) 2894-2906.
[36] Y. Gao, Y. Liu, L. Zhou, Z.H. Guo, M.D. Rong, X.N. Liu, C.H. Lai, X.L. Ding, The Effects of Different Wavelength UV Photofunctionalization on Micro-Arc Oxidized Titanium, Plos One, 8 (2013).

583 [37] H.P. Erickson, N. Carrell, J. Mcdonagh, Fibronectin Molecule Visualized in Electron-
584 Microscopy - a Long, Thin, Flexible Strand, Journal of Cell Biology, 91 (1981) 673-678.
585 [38] V.E. Koteliansky, M.A. Glukhova, M.V. Bejanian, V.N. Smirnov, V.V. Filimonov,
586 O.M. Zalite, S.Y. Venyaminov, A Study of the Structure of Fibronectin, European Journal of
587 Biochemistry, 119 (1981) 619-624.
588 [39] A.K. Wright, M.R. Thompson, Hydrodynamic Structure of Bovine Serum-Albumin
589 Determined by Transient Electric Birefringence, Biophysical Journal, 15 (1975) 137-141.
590 [40] E. Anbazhagan, A. Rajendran, D. Natarajan, M.S. Kiran, D.K. Pattanayak, Divalent ion
591 encapsulated nano titania on Ti metal as a bioactive surface with enhanced protein adsorption,
592 Colloids and Surfaces B-Biointerfaces, 143 (2016) 213-223.
593 [41] D.H. Shin, T. Shokuhfar, C.K. Choi, S.H. Lee, C. Friedrich, Wettability changes of TiO2
594 nanotube surfaces, Nanotechnology, 22 (2011).
595 [42] J. Guo, R.J. Padilla, W. Ambrose, I.J. De Kok, L.F. Cooper, The effect of hydrofluoric
596 acid treatment of TiO2 grit blasted titanium implants on adherent osteoblast gene expression
597 in vitro and in vivo, Biomaterials, 28 (2007) 5418-5425.
598 [43] M. Kulkarni, Y. Patil-Sen, I. Junkar, C.V. Kulkarni, M. Lorenzetti, A. Iglic, Wettability
599 studies of topologically distinct titanium surfaces, Colloids and Surfaces B-Biointerfaces,
600 129 (2015) 47-53.
601 [44] I. Junkar, M. Kulkarni, B. Drasler, N. Rugelj, N. Recek, D. Drobne, J. Kovac, P.
602 Humpolicek, A. Iglic, M. Mozetic, Enhanced biocompatibility of TiO2 surfaces by highly
603 reactive plasma, Journal of Physics D-Applied Physics, 49 (2016).
604 [45] E. Gongadze, D. Kabaso, S. Bauer, T. Slivnik, P. Schmuki, U. van Rienen, A. Iglic,
605 Adhesion of osteoblasts to a nanorough titanium implant surface, Int J Nanomedicine, 6
606 (2011) 1801-1816.
607

608

Figure S1

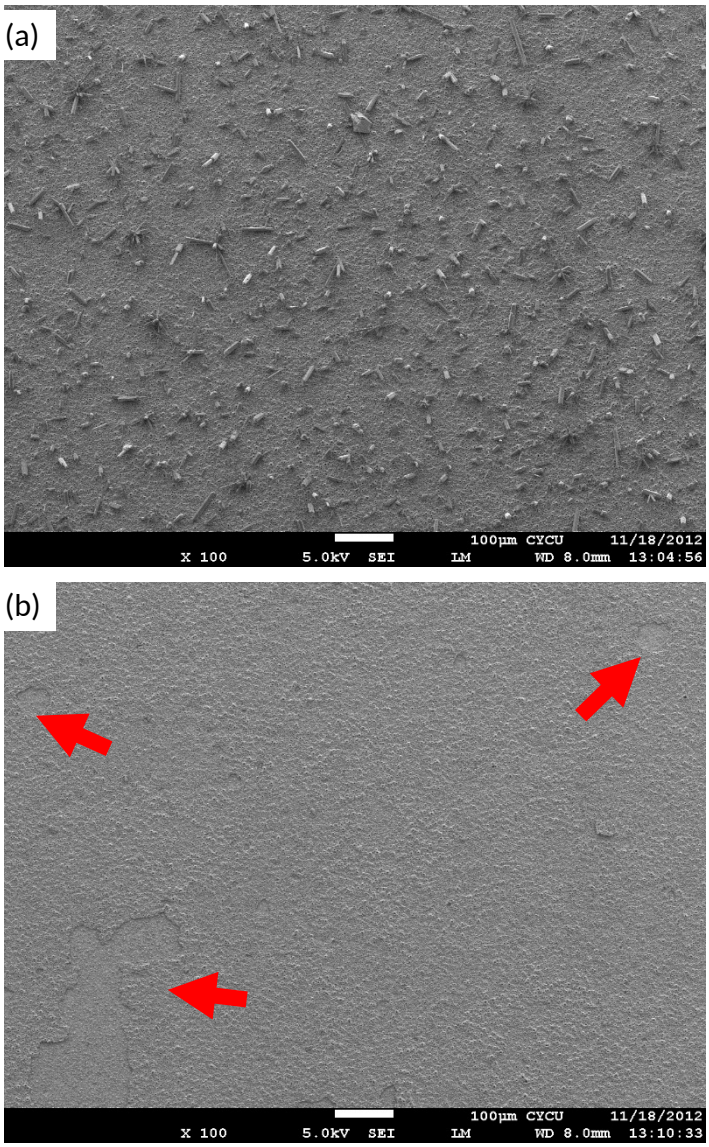

Figure S1

The morphology of HT sample before (a) and after (b) the sonicated clean in DD water for 30 minutes. The HA precipitates peered off and the MAO layer was de-lamellar (red arrows) during the cleaning process.

Table S1 Adherent cell number and spreading percentage of MG63 cells on the samples after cultured for 4 hr.

Sample codes	Cell adherent and spreading	
	Total cell number*	Percentage of spreading
MAO	245.0 ± 74.7	48.4%
HT	175.4 ± 44.2	41.5%
MWDD	280.6 ± 84.1	75.7%
MWCP	296.8 ± 84.8	69.9%
MWCP9	290.0 ± 33.6	69.4%
MWCP11	240.2 ± 18.2	72.5%

*Total cell number in five 100X picture taken from different location on samples.